Improved InxGa1_xP/GaAs /Ge tandem solar cell using light trapping engineering and multi-objective optimization approach

https://doi.org/10.1016/j.ijleo.2020.165346

# Improved $In_xGa_{1\_x}P$/GaAs /Ge tandem solar cell using light trapping engineering and multi-objective optimization approach

H. Bencherif [1,*], L. Dehimi[1,2], F. Pezzimenti[3], A. Yousfi[4], M.A. Abdi[5,6], L. Saidi[4], F. G. Della Corte[3]

[1]LMSM, Department of Physics University of Biskra, Biskra, Algeria.
[2]Faculty of Material Science, University of Batna , Algeria
[3]-DIIES, Mediterranea University of Reggio Calabria, Reggio Calabria, Italy.
[4] LAAAS, Department of Electronics, University Batna 2, Algeria.
[5] LEPCM, Laboratory of Physico-chemical Study of Materials, University of Batna1, 05000, Algeria
[6]Faculty of Technology, University of Batna2, 05000, Algeria

* Corresponding author. E-mail address: hichem.bencherif@univ-batna2.dz (H. Bencherif)

## Abstract

In this paper, an analytical model for studying the effect of light trapping mechanism on tandem solar cell performance is developed. The proposed model considers diffraction grating morphology and antireflection coating of the $In_xGa_{1\_x}P$/GaAs /Ge tandem solar cell. The main photovoltaic figures of merit of the $In_xGa_{1\_x}P$/GaAs /Ge tandem solar cell are investigated. The obtained results prove the outstanding capability of the light trapping mechanism to improve device performance. An efficiency of 32.5% was obtained. A short circuit current of ($J_{SC}$ =28 mA/cm$^2$), the open-circuit voltage of ($V_{OC}$ =1.288V), and a fill factor of ($FF$=87.7%) were distinguished. In addition, the developed model serves as a fitness function to optimize the light trapping capability using a multi-objective particle swarm optimization (MOPSO) approach. The optimized tandem solar cell design exhibits higher performance in terms of short circuit current density ($J_{SC}$=35.3 mA/cm$^2$) and open-circuit voltage ($V_{OC}$ =1.305 V). Besides, an efficiency of 41.7% is obtained which outweighs that of the conventional planar solar cell. Therefore, the proposed design methodology efficiently minimize the reflectance via establishing an intensive light trapping mechanism at the front of both sub-cells and opens promising opportunities to enhance the tandem solar cell performances.

**Keywords:** Tandem solar cells**,** InGaP/GaAs, Analytical model, light trapping, MOPSO approach.

https://doi.org/10.1016/j.ijleo.2020.165346

## 1. Introduction

Nowadays, the suitable structure to reach higher photovoltaic conversion efficiency is generally obtained from multi-junction solar cells based on III–V semiconductors [1]. Tandem solar cells made of III-V semiconductor materials are recognized as a paved way to reach a high conversion efficiency, this is due mainly to the wide range of absorption in the solar spectrum [2-4]. To improve the solar cell optical performances, several efforts focused on optimizing the solar cell structure, technological process, and the quality of the epitaxial layer [5-8]. Among these attempts, the deposition of nanoparticles on the solar cell surface improves the conversion efficiency remarkably [9]. Besides, the texturing process has become a vital step in solar cell fabrication, where the roughed surface assures a destructive interference that enhances the device transmittance [10]. Although, the recorded conversion efficiency of 40.8% was stated [11], optimizing the solar cell efficiency is still costly and time-consuming when dealing with experiments. To reduce the dilemma faced according to the experimental optimization of the dual-junction tandem solar cell structures, the development of an accurate analytical model is recommended. Herein, we propose an analytical model account for a single layer antireflection coating (*SLARC)* and textured subcells front surface to improve the tandem solar cell conversion efficiency. Moreover, a back surface field layer is incorporated to enhance the collection mechanism of the photo-generated carriers. The light trapping and the BSF design parameters effect on the device performances are investigated via the developed analytical model. That is used as a fitness function for a Multi-Objective Particle Swarm Optimization approach (MOPSO) to locate the optimal parameters combination of light trapping formalism. The adopted methodology conducts to maximum conversion efficiency [12-15]. The generality of the obtained result suggests that the proposed design methodology based on the combined light trapping engineering and multiobjective optimization approach will have potential applications in future solar cells.

https://doi.org/10.1016/j.ijleo.2020.165346

## 2. Device structure

The proposed solar cell structure shown in figure 1 consists of a thin top cell ($In_{0.49}Ga_{0.51}P$/GaAs) stacked on a Ge bottom cell separated by an adhesive layer. The penetration of light through the structure is depending on materials band gaps.

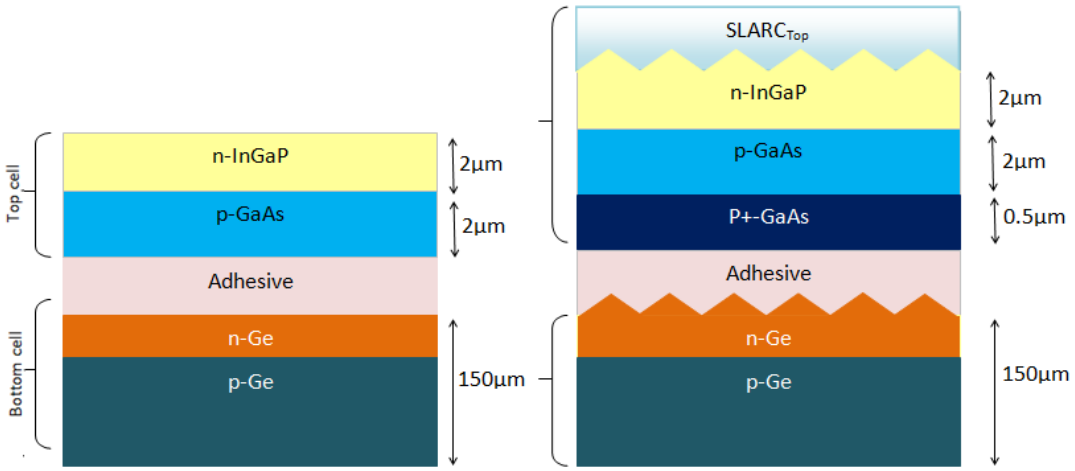


**(a)** **(b)**

**Figure.1** Cross-sectional view of the investigated solar cell (a) Conventional tandem solar cell (b) Proposed tandem solar cell with BSF layer and interfaces texture morphology. (2-terminal device).

In this paper we adopt diffraction grating morphology for the sake of ensuring an intensive injection of light. The proposed geometrical formalism is sufficient for trapping the greater part of the light into the solar cell. Additionally, a single layer antireflection coating (*SLARC)* and back surface field (BSF) layers are used.

## 3. Analytical Model

### 3.1 Modeling of the reflected incident light

The cross-sectional view of the diffraction grating engineering used in the investigated TJSC (Tandem Junction Solar Cell) surfaces is plotted in Figure 2.

https://doi.org/10.1016/j.ijleo.2020.165346

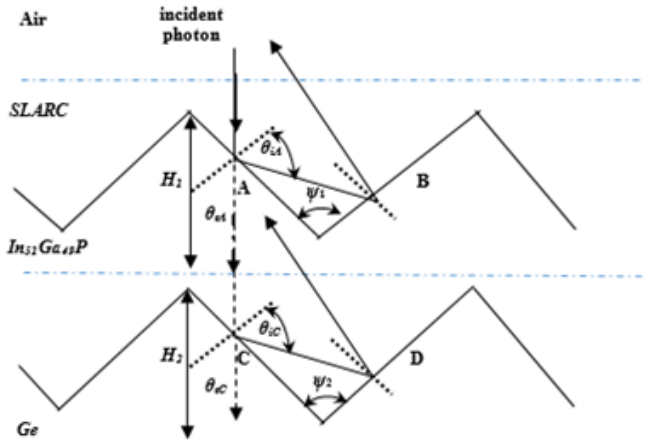


**Figure.2** Schematic representation of the ray propagation through different layers

All the geometrical parameters of the proposed shape are illustrated in this figure. where $\theta_{iA}$ denotes the angle of incident beam on the wall *A*. $\psi_1$, $\psi_2$, $H_1$ and $H_2$ represent, respectively, the angles and heights of the pyramid textures formalism.

The coefficient of absorption $\alpha(\lambda)$ for flat surfaces is calculated via the standard expression $\alpha(\lambda)=\frac{B}{E}\left(E-E_g\right)^{\frac{1}{2}}$ , where $E$ and $E_g$ represent, the photon energy and energy bandgap respectively, $B$ is a physical parameter relates to the type of material.

Among optical parameters metrics, the reflection coefficient is an efficient factor to quantify the optical losses in the investigated TJSC.

The reflection coefficient considering the texturization morphology can be calculated for both sub cells as follows [16, 17]:

$$R=\frac{r_{12}^{\,2}+r_{23}^{\,2}+2r_{12}r_{23}\cos(2\beta)}{1+r_{12}^{\,2}r_{23}^{\,2}+2r_{12}r_{23}\cos(2\beta)} \quad (1)$$

$$\beta=\frac{2\pi n_i d}{\lambda} \quad (1\text{-a})$$

where $d$ denotes the anti-reflection coating thickness. $n_1$ , $n_2$ and $n_3$ represent the refractive indices for Air/ARC/InGaP ($i$=*1-3*).

The coefficients $r_{12}$ and $r_{23}$ denote, the partial reflection coefficients, for air, *ARC* and *InGaP*

https://doi.org/10.1016/j.ijleo.2020.165346

layers, respectively. The partial reflection coefficient between air and *ARC* layers is calculated by [18]:

$$r_{12} = \frac{n_2 - n_1}{n_2 + n_1} \quad (2)$$

The coefficient, $r_{23}$, that describes the diffracted beam at the pyramid walls (ARC/ *InGaP*), is expressed using Fresnel equations as follows [19]:

$$r_{23} = \frac{R\parallel + R\perp}{2} = \frac{R_{A\parallel}R_{B\parallel} + R_{A\perp}R_{B\perp}}{2} \qquad (3)$$

where $R_{A\parallel}R_{B\parallel} and R_{A\perp}R_{B\perp}$ are given by Fresnel equations as,

For parallel component:

$$R_{A\parallel} = \frac{n_3\cos\theta_{iA} - n_2\cos\theta_{tA}}{n_3\cos\theta_{iA} + n_2\cos\theta_{tA}} \qquad (4a) \qquad R_{B\parallel} = \frac{n_3\cos\theta_{iB} - n_2\cos\theta_{tB}}{n_3\cos\theta_{iB} + n_2\cos\theta_{tB}} \qquad (4b)$$

For perpendicular component:

$$R_{\mathrm{A}\perp} = \frac{n_2\cos\theta_{iA} - n_3\cos\theta_{tA}}{n_2\cos\theta_{iA} + n_3\cos\theta_{tA}} \qquad (5a) \qquad R_{\mathrm{B}\perp} = \frac{n_2\cos\theta_{iB} - n_3\cos\theta_{tB}}{n_2\cos\theta_{iB} + n_3\cos\theta_{tB}} \qquad (5b)$$

After a mathematical manipulation we get the following expression of the incident and transmission angles of the proposed top sub cell design (figure 2):

$$\theta_{iB} = \psi - \theta_{iA} \qquad (6a)$$

$$\theta_{tA} = \sin^{-1}\left(\frac{1}{n_{23}}\sin\theta_{iA}\right) \quad (6b)$$

$$\theta_{tB} = \sin^{-1}\left(\frac{1}{n_{23}}\sin\theta_{iB}\right) \quad (6c)$$

With $n_{23} = \frac{n_3}{n_2}$

In the previous expressions, the subscripts *t* and *i* represent, the transmitted and incident light beams, respectively. The same procedure is adopted to model the reflection coefficient considering the texture morphology of the bottom sub cell.

https://doi.org/10.1016/j.ijleo.2020.165346

By considering the incident beam path in the different textured sub cells, the absorption coefficient is calculated using the following expressions [20].

For top sub cell: $$\overline{\alpha}_{textured\ top} = \frac{\alpha_{top\ flat}}{\cos\theta_{tA}} \qquad (7\text{-a})$$

For bottom sub cell: $$\overline{\alpha}_{textured\ bottom} = \frac{\overline{\alpha}_{textured\ top}}{\cos\theta_{tA\ bottom}} \qquad (7\text{-b})$$

### 3.2 photocurrent modeling

The total current density ($J_{Total}$) of the investigated TJSC solar cell is expressed as follows [21]:

$$J_{Total} = J_L - J_0\left[e^{\frac{qv}{kT}} - 1\right] \qquad (8)$$

where $J_0$ refers to the saturation current of both sub-cells [21]. $J_L$ represent the photogenerated carriers current. It is worth of noticing that $J_L$ is dependent on the optical properties of the TJSC constituted material. The latter is the summation of the photo generated carriers currents in the emitter, base, and depletion region. $J_L$ can be calculated as

$$J_L = \int_{\lambda_{\min}}^{\lambda_{\max}} q \times F(\lambda) \times SR(\lambda) d\lambda \qquad (9)$$

where $F$ denotes the flux of the incident beam, $\lambda$ and $q$ are, the incident photon wavelength and the electron charge , respectively, $\lambda_{min}$ and $\lambda_{max}$ represent, the minimum and maximum (cut-off) wavelength, respectively .The later relates to the bandgap energy.

At the end, we consider the spectral response $SR(\lambda)$ as the summation of the contributions of fundamental regions, i.e.

$$SR(\lambda) = SR_{Emitter}(\lambda) + SR_{Depletedreg}(\lambda) + SR_{Base}(\lambda) \qquad (10)$$

The $SR(\lambda)$ express the light conversion capability to a current. Considering the top cell structure $In_{0.49}Ga_{0.51}P$/GaAs, the $SR(\lambda)$ can be calculated as follows [21]:

https://doi.org/10.1016/j.ijleo.2020.165346

$$SR_{Emitter} = \left[\frac{q(1-R)\alpha_{InGaP}L_P}{\alpha_{InGaP}^2 L_p^2 - 1}\right] \times \left[\frac{\left(\frac{S_p L_p}{D_p} + \alpha_{InGaP}L_p\right) - e^{-\alpha_{InGaP}y_1}\left(\frac{S_p L_p}{D_p}\cosh\frac{y_1}{L_p} + \sinh\frac{y_1}{L_p}\right)}{\left(\frac{S_p L_p}{D_p}\sinh\frac{y_1}{L_p} + \cosh\frac{y_1}{L_p}\right)} - \alpha_{InGaP}L_p e^{-\alpha_{InGaP}y_1}\right] \quad (11)$$

$$SR_{Base} = \left[\frac{q(1-R)\alpha_{GaAs}L_n}{\alpha_{GaAs}^2 L_n^2 - 1}\right] \times e^{-\alpha_{GaAs}y_3} \times \left[\alpha_{GaAs}L_n - \frac{\frac{S_n L_n}{D_n}\left(\cosh\frac{y_4 - y_3}{L_n} - e^{-\alpha_{GaAs}(y_4 - y_3)}\right) + \sinh\frac{y_4 - y_3}{L_n} + \alpha_{GaAs}L_n e^{-\alpha_{GaAs}(y_4 - y_3)}}{\left(\frac{S_n L_n}{D_n}\sinh\frac{y_4 - y_3}{L_n} + \cosh\frac{y_4 - y_3}{L_n}\right)}\right] \quad (12)$$

$$SR_{Depleted\ reg} = q(1-R)\left(e^{-\alpha InGaP y_1} - e^{-\alpha InGaP y_2} - e^{-\alpha GaAs(y_3 - y_2)}\right) \quad (13)$$

where $y_i$ *(i=1-4)*denotes the physical thickness of the fundamental region of the top sub cell accounting for the excursion of the depletion width. $S_{n\ (p)}$ refers to the electrons (holes) surface recombination velocity, and $L_{n\ (p)}$ denotes the electrons (holes) diffusion length. The latter can be calculated via the following expression:

$$L_{p,n} = \sqrt{D_{p,n} \times \tau_{p,n}} \quad (14)$$

Here, $\tau_{n(p)}$is the electrons (holes) lifetime, and $D_{n\ (p\ )}$is the electrons (holes) diffusion constant given by the Einstein's relation as

$$D_{p,n} = \frac{k \times T}{q}\mu_{p,n} \quad (15)$$

where *k* represent the constant of Boltzmann, *T* refers to the temperature. $\mu_{n\ (p)}$ is the electrons (holes) mobility $\alpha_{InGaP}$ and $\alpha_{GaAs}$ denote the absorption coefficients of emitter region (InGaP) and base region (GaAs), respectively.

Alike, the Ge bottom cell the spectral response is modeled [21].

https://doi.org/10.1016/j.ijleo.2020.165346

$$SR_{Emitter}=\left[\frac{q(1-R^{'})\alpha_{Ge}L_{P}}{\alpha_{Ge}^{2}L_{p}^{2}-1}\right]\times\left[\frac{\left(\frac{S_{p}L_{p}}{D_{p}}+\alpha_{Ge}L_{p}\right)-e^{-\alpha_{Gey_{1}^{'}}}\left(\frac{S_{p}L_{p}}{D_{p}}\cosh\frac{y_{1}^{'}}{L_{p}}+\sinh\frac{y_{1}^{'}}{L_{p}}\right)}{\left(\frac{S_{p}L_{p}}{D_{p}}\sinh\frac{y_{1}^{'}}{L_{p}}+\cosh\frac{y_{1}^{'}}{L_{p}}\right)}-\alpha_{Ge}L_{p}e^{-\alpha_{Gey_{1}^{'}}}\right] \quad (16)$$

$$SR_{Base}=\left[\frac{q(1-R^{'})\alpha_{Ge}L_{n}}{\alpha_{Ge}^{2}L_{n}^{2}-1}\right]\times e^{-\alpha_{Ge}y_{3}^{'}}\times \left[\alpha_{Ge}L_{n}-\frac{\frac{S_{n}L_{n}}{D_{n}}\left(\cosh\frac{y_{4}^{'}-y_{3}^{'}}{L_{n}}-e^{-\alpha_{Ge}(y_{4}^{'}-y_{3}^{'})}\right)+\sinh\frac{y_{4}^{'}-y_{3}^{'}}{L_{n}}+\alpha_{Ge}L_{n}e^{-\alpha_{Ge}(y_{4}^{'}-y_{3}^{'})}}{\left(\frac{S_{n}L_{n}}{D_{n}}\sinh\frac{y_{4}^{'}-y_{3}^{'}}{L_{n}}+\cosh\frac{y_{4}^{'}-y_{3}^{'}}{L_{n}}\right)}\right] \quad (17)$$

$$SR_{Depletedreg}(\lambda)=q(1-R^{'})\times e^{-\alpha GeY_{1}^{'}}\times(1-e^{-\alpha Ge(Y_{3}^{'}-Y_{1}^{'})}) \quad (18)$$

where $\alpha_{Ge}$ represents Germanium absorption coefficient.

In order to consider the BSF layer contribution, we incorporate into the model an effective surface recombination velocity $S_{e,\,pp+}$ in the place of the front cell surface recombination velocity $S_{n.}$. The effective surface recombination velocity is calculated by solving the 2D continuity equation in dark condition for highly doped GaAs and expressed as follows [22]:

$$S_{e,pp}=\frac{N_{a}D_{n}^{+}}{N_{a}^{+}L_{n}^{+}}\frac{\frac{S_{n}L_{n}^{+}}{D_{n}^{+}}\cosh\left(\frac{W_{BSF}}{L_{n}^{+}}\right)+\sinh\left(\frac{W_{BSF}}{L_{n}^{+}}\right)}{\cosh\left(\frac{W_{BSF}}{L_{n}^{+}}\right)+\frac{S_{n}L_{n}^{+}}{D_{n}^{+}}\sinh\left(\frac{W_{BSF}}{L_{n}^{+}}\right)} \quad (19)$$

where $N_a$, $L_n^+$and $D_n^+$ refer, respectively, to the doping concentration in base, the diffusion length and the diffusion constant. $N_a^+$ and $W_{BSF}$ are the *BSF* layer's doping concentration and thickness, respectively. The effect of the design parameters on the solar cell output performances such as fill factor and conversion efficiency can be examined adopting the following equations:

https://doi.org/10.1016/j.ijleo.2020.165346

$$FF(R) = \frac{P_m(R)}{J_{SC}(R)V_{OC}(R)} \quad (20a) \qquad \eta(R) = \frac{P_m(R)}{P_i} \quad (20b)$$

where $J_{SC}$, $P_m$, and $V_{OC}$ denote the short circuit current, maximum power, and open circuit voltage. $P_i$ denotes the incident power. The $In_{0.49}Ga_{0.51}P$/GaAs/Ge tandem solar cell structure physical and geometrical parameters are mentioned in Table 3.

**Table.3** Geometrical and physical parameters of the TJSC.

| Parameters | InGaP | GaAs | Ge (n-type) | Ge (p-type) |
|---|---|---|---|---|
| $y_1$ (µm) | 0.1 | / | 0.2 | / |
| $Y_2$ (µm) | 2 | / | | |
| $y_4$-$y_2$ (µm) | / | 2 | | |
| $N_d$ ($cm^{-3}$) | $5\times10^{13} - 1\times10^{18}$ | / | $1\times10^{16} - 1\times10^{19}$ | / |
| $N_a$ ($cm^{-3}$) | / | $5\times10^{18}$ | / | $1\times10^{18}$ |
| $S_p$ (cm/s) | $5\times10^{13} - 1\times10^{18}$ | / | $1\times10^{5} - 1\times10^{6}$ | / |
| $S_n$ (cm/s) | / | $1\times10^{5}$ | / | $1\times10^{6}$ |

## 4. Results and discussions

### 4.1. Textured $In_{0.49}Ga_{0.51}P$/GaAs Top Cell with ARC

Figure 3 shows the calculated conversion efficiency of $In_xGa_{1\_x}P$/GaAs top cell using several *In* mole fractions.

From figure 3, It is observed that increasing the *In* mole fraction leads to an improvement in the solar cell efficiency. As an example, for a 590 nm wavelength the efficiency reaches a 33.5%, 34.5% and 36.7% for *In* mole fraction values of 0.5, and 0.6 and 0.7. Besides, the $V_{OC}$ decrease when increasing In mole fraction, this fact is linked to the rise of saturation current caused by the minimized Schottky barrier. The enhancement in the efficiency is mainly attributed to the decreased band gap energy leading to an improved absorption coefficient.

The tuning of the refractive index of the *ARC* layer plays a crucial role in improving the proposed TJSC optical output parameters. Therefore, the study of the impact of this parameter remains indispensable and must be carried out. In this framework, the *ARC's* refractive index was varied in the range of {1-4}. Figure.4 shows the electrical output parameters of the top sub cell as function of *ARC* refractive index.

https://doi.org/10.1016/j.ijleo.2020.165346

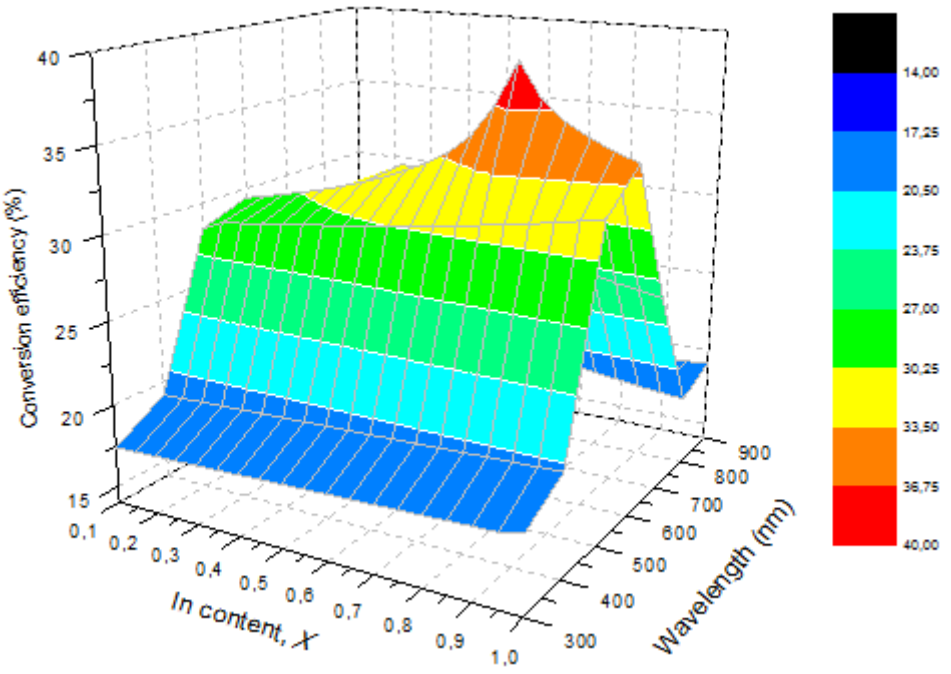


**Figure.3** The conversion efficiency of $In_xGa_{1-x}P/GaAs$ top cell as function of wavelength for different *In* content values ($d=30nm$, $n=1.6$, $\psi_1=1.2$ rad, $N_{A\text{-}GaAs}=10^{16}\ cm^{-3}$, $N_{D\text{-}InGaP}=10^{18}\ cm^{-3}$, $N_{A\text{-}BSF}=10^{19}$).

https://doi.org/10.1016/j.ijleo.2020.165346

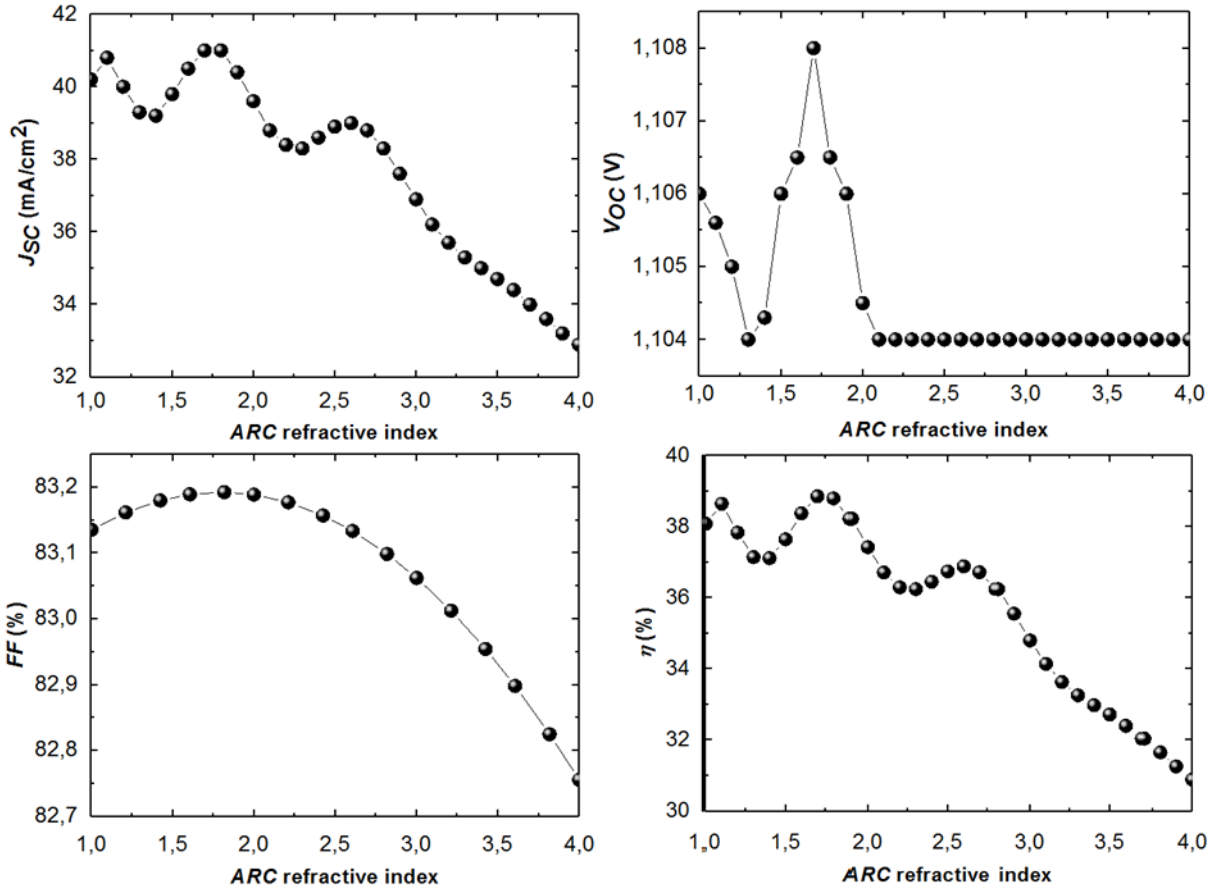


**Figure.4** The electrical outputs of the $In_xGa_{1-x}P/GaAs$ top cell as function of *ARC* refractive index ($d=30nm$, $\psi_1=1.2$ rad, $N_{A\text{-}GaAs}=10^{16}$ $cm^{-3}$, $N_{D\text{-}InGaP}=10^{18}$ $cm^{-3}$, $N_{A\text{-}BSF}=10^{19}$).

From this figure it is obvious that the efficiency is affected by variation of the refractive index. This fact is attributed to the direct influence of this parameter on absorption and transmission coefficients which improves the short circuit current at a specific range. By accurately choosing the *ARC* refractive index, the reflected light of a range of wave lengths can interfere destructively, lowering reflectance. On the other hand, the values of $V_{oc}$ and *FF* of the sub cell have risen slightly. An optimum efficiency is occurring in a refractive index equal to 1.8. The surface texturization is used to decrease the reflectivity of the solar cell surface. This operation aims to create a surface roughness. The most common method used to achieve surface texturization is a chemical attack (KOH) creating pyramid-shaped roughness (with characteristic dimensions ranging from 5 to 10 μm) [23]. Figure 5 shows the influence of the angle of texturization on the electrical figures of merit of the top cell.

https://doi.org/10.1016/j.ijleo.2020.165346

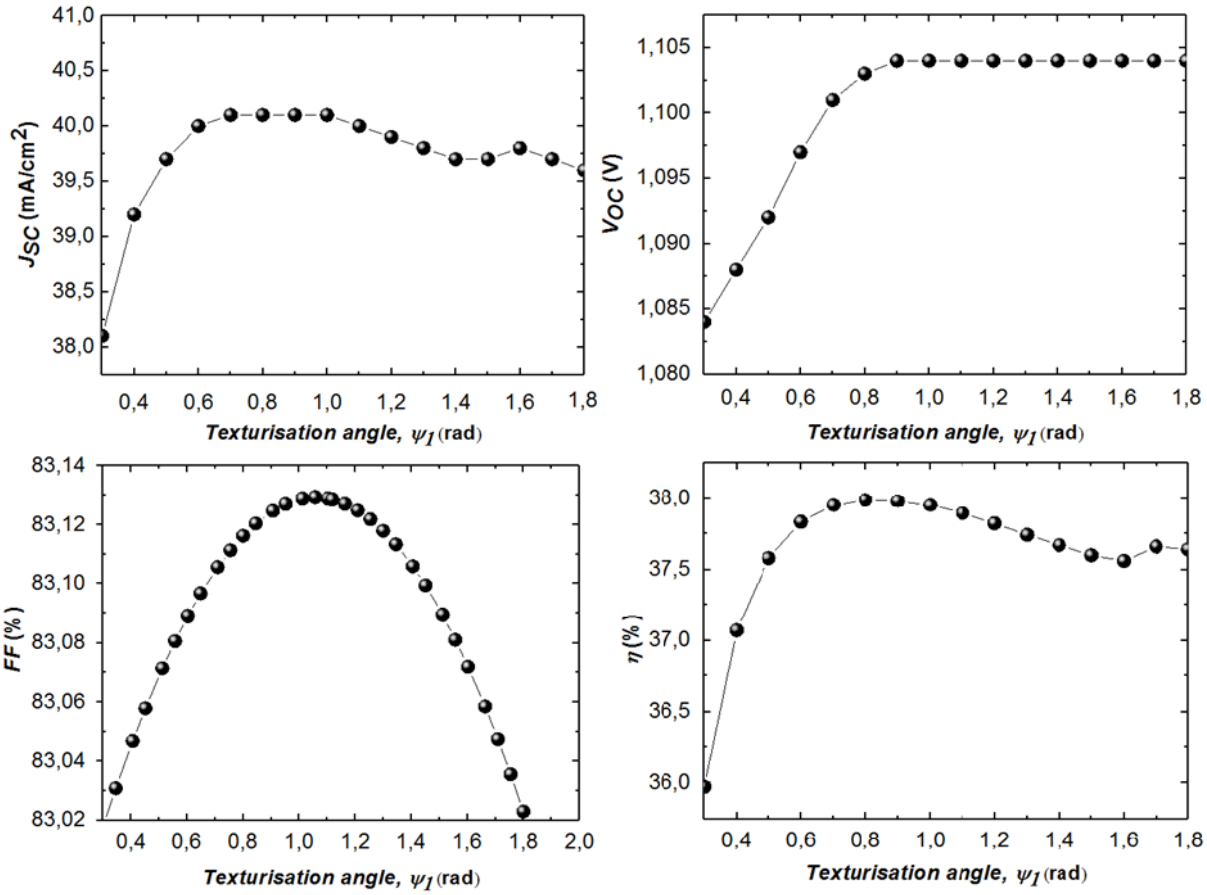


**Figure.5** The electrical outputs of the $In_xGa_{1-x}P/GaAs$ top cell as function of the angle of texturization ($d=30nm$, $n=1.6$, $N_{A\text{-}GaAs}=10^{16}\ cm^{-3}$, $N_{D\text{-}InGaP}=10^{18}\ cm^{-3}$, $N_{A\text{-}BSF}=10^{19}$).

It is observed from this figure, that for a texturization angle equal to 0.8 rad the short circuit current increases to a value of 40.2V, this is mainly attributed to the mechanism of light trapping activated at the surface area. As shown in Figure 6, a slight change in the $V_{OC}$ is observable.

The Back Surface Field (*BSF*) is technique for minimizing the influence of surface recombination. The creation of a potential barrier (for example, p+/p junction) on the solar cells back ensures high collection of photo-generated carriers. Figure 6 shows a comparison of the *J-V* characteristics between the proposed top sub cell with and without BSF layer and the conventional design.

https://doi.org/10.1016/j.ijleo.2020.165346

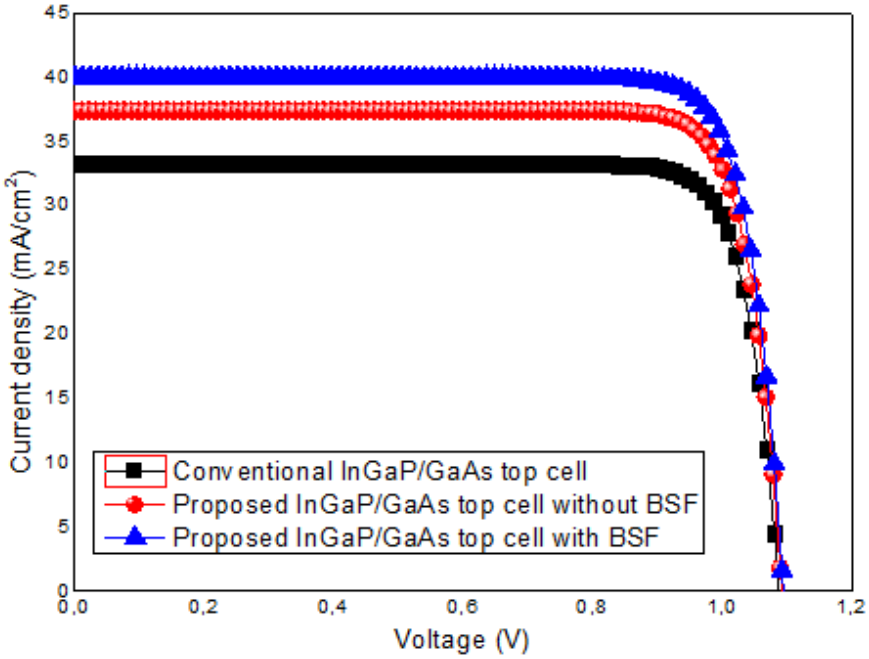


**Figure.6** Comparison between conventional and proposed $In_{0.49}Ga_{0.51}P$/GaAs top sub cells with and without BSF layer. ($d=30nm$, $n=1.6$, $\psi_1=1.2$ rad, $N_{A\text{-}GaAs}=10^{16}$ $cm^{-3}$, $N_{D\text{-}InGaP}=10^{18}$ $cm^{-3}$, $N_{A\text{-}BSF}=10^{19}$).

As shown in figure. 6, the proposed top sub cell including BSF layer outperforms the conventional solar cells in terms of short circuit current ($J_{SC}$). This improvement is mainly due to the role of BSF layer in reducing the carrier's loss at the rear side. Table 4 summarizes the obtained results.

**Table.4** Electrical output parameters of proposed and conventional top sub cells

| Parameters | $J_{SC}$(mA) | $V_{oc}$(V) | *FF* (%) | *Pm* ($mW/cm^2$) | $\eta$ (%) |
|---|---|---|---|---|---|
| **Conventional top cell** | 33.3 | 1.09 | 83.8 | 30.43 | **31.3** |
| **Proposed top cell without BSF** | 37.4 | 1.09 | 84.23 | 34.34 | **35.3** |
| **Proposed top cell with BSF** | 40 | 1.09 | 84.3 | 36.77 | **38** |

### 4.2.Textured Ge bottom cell

The bottom solar cell structure physical and geometrical parameters are mentioned in Table 3. With the aim of reducing the unwanted reflection, a bottom sub cell with diffraction grating morphology has been proposed. Figure 7 shows the investigated solar cell figures of merit as function of texturization angle.

https://doi.org/10.1016/j.ijleo.2020.165346

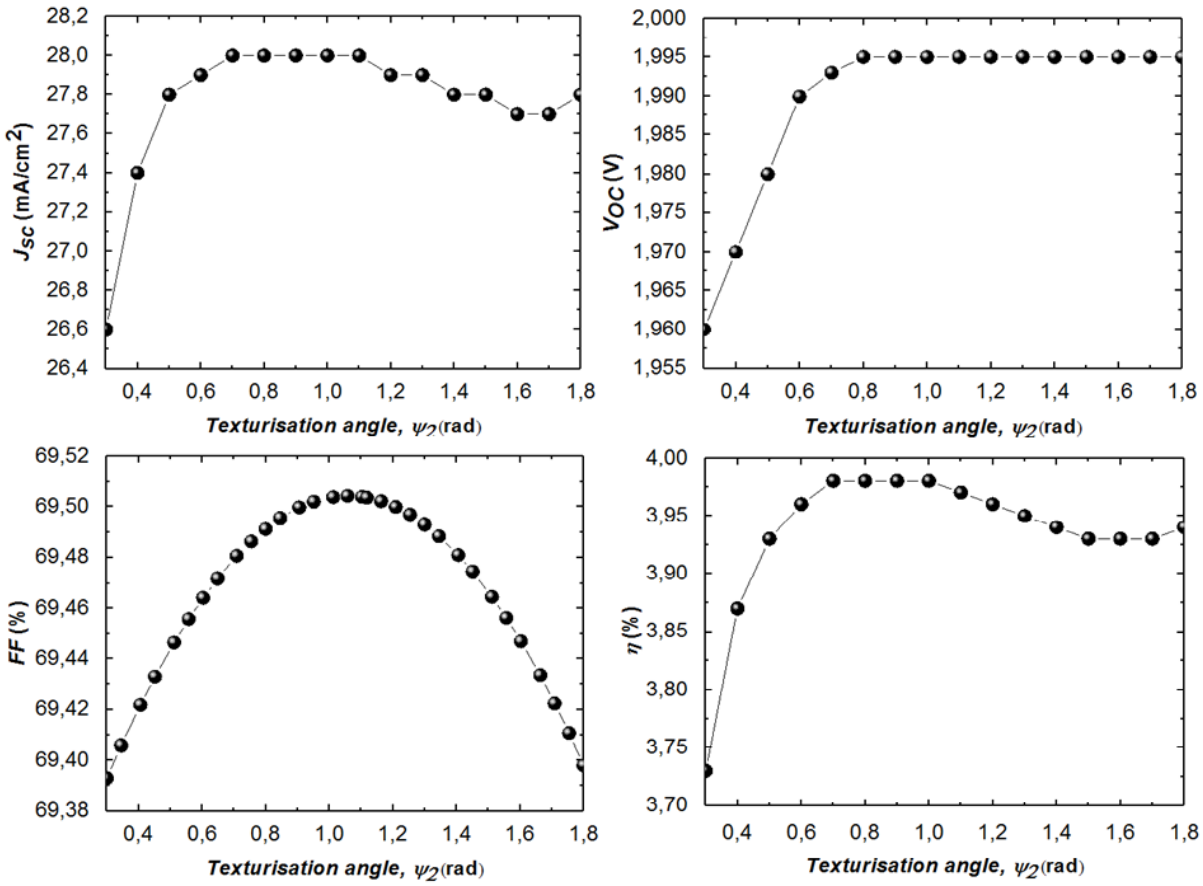


**Figure.7** The electrical outputs of Ge bottom solar cell as function of the angle of texturization (*d=30nm, n=1.6*, $\psi_1$*=1.2 rad,* $N_{A\text{-}GaAs}=10^{16}$ *cm*$^{-3}$, $N_{D\text{-}InGaP}=10^{18}$ *cm*$^{-3}$, $N_{A\text{-}BSF}=10^{18}$).

From figure 7 it is obvious that the solar cell has a maximum electrical output when the angle of texturization is around 1.2 rad, where the $J_{SC}$ is equal to 28 mA/cm$^2$ and the conversion efficiency is around 3.96 %. This enhancement is due mainly to the good surface control via light trapping design which permits to capture a large amount of light. The *J(V)* and *P(V)* characteristics of the proposed and conventional Ge bottom sub cell are shown in Figure 8.

https://doi.org/10.1016/j.ijleo.2020.165346

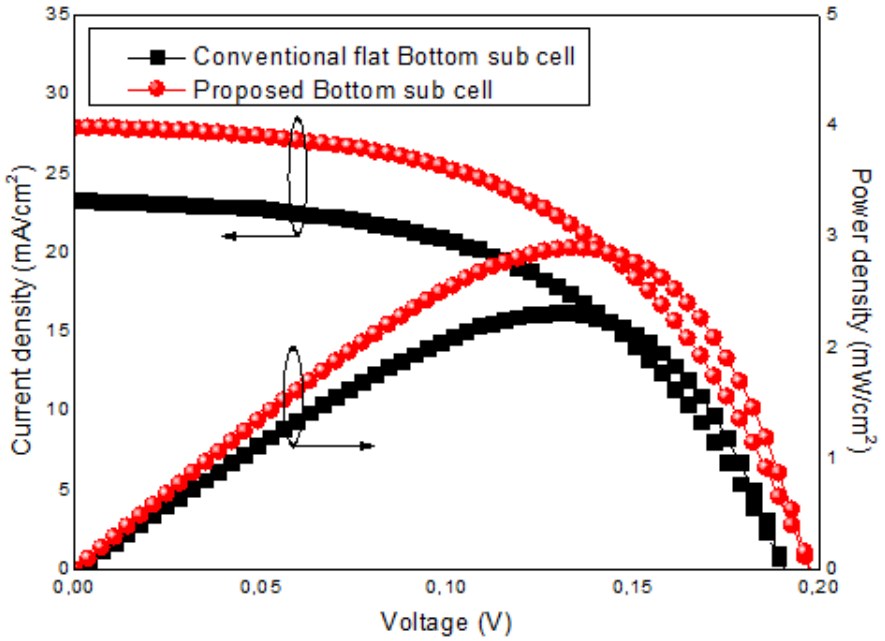


**Figure.8** *J-V* and *P-V* characteristics of the proposed and conventional Ge bottom cell at T = 300 K ($d=30nm$, $n=2$, $\psi_1=1.2$ rad, $\psi_2=1.2$ rad , $N_{A\text{-}Ge}=10^{16}$ $cm^{-3}$, $N_{D\text{-}Ge}=10^{19}$ $cm^{-3}$).

From figure 8 it is observed that the proposed design with surface texturization surpasses the conventional design, where an improvement of 16.7% and 4% in terms of $J_{SC}$ and $V_{OC}$ is obtained. The obtained results are summarized in table 5.

**Table.5** Electrical output parameters of the conventional and proposed bottom sub cell.

| Parameters | $J_{SC}$(mA) | $V_{oc}$(V) | *FF* (%) | *Pm* ($mW/cm^2$) | $\eta$ (%) |
|---|---|---|---|---|---|
| **Conventional bottom sub cell** | 23.3 | 0.19 | 52.4 | 2.32 | **3.16** |
| **Proposed bottom sub cell** | 28 | 0.198 | 52.3 | 2.9 | **3.96** |

https://doi.org/10.1016/j.ijleo.2020.165346

### 4.3.Boosting up the tandem solar cell performances using MOPSO approach

The MOPSO is a metaheuristic approach based on mimicking the natural bird swarm behavior. This method can be formulated by populations $P_t$ that constituted from $N$ particles for $t$ generations in the random space $S$ [24-25].

The particle position is expressed as follows:

$$\vec{x}^i = x_1^i, x_2^i, ...x_n^i \qquad (21)$$

and the particle velocity is:

$$\vec{v}^i = v_1^i, v_2^i, ...v_n^i \qquad (22)$$

The position and velocity of the particle are updated for the next generation as:

$$v_{j,t+1}^i = wv_{j,t}^i + c_1R_1(p_{j,t}^i - x_{j,t}^i) + c_2R_2(p_{j,t}^{i,g} - x_{j,t}^i) \qquad (23)$$

$$x_{j,t+1}^i = x_{j,t}^i + v_{j,t}^i \qquad (24)$$

where $w$ represents the particle inertia weight, $R_1$ and $R_2$ denote the randomly generated value in the range of (0, 1), respectively. And $c_1$ and $c_2$ represent positive constants. The ultimate step in this approach is to locate the superior (best) global particle $\vec{p}_t^{i,g}$ of the population. Knowing that a multiobjective optimization criterion generates a multitude of Pareto solutions (optimum), therefore, a single Pareto solution is chosen by each particle as a global optimum particle. For the next iterations, particles will be updated and assessed, and then the non dominated ones will be excluded. The MOPSO approach repeats iteratively the optimization procedure. The steps of a MOPSO keep reiterating till it reaches the stopping criteria [26-28].

In this work, we use the MOPSO approach to optimize the structure of tandem solar cell via improving the light trapping and BSF capability. The flow chart for the proposed MOPSO approach is shown in Figure 9.

https://doi.org/10.1016/j.ijleo.2020.165346

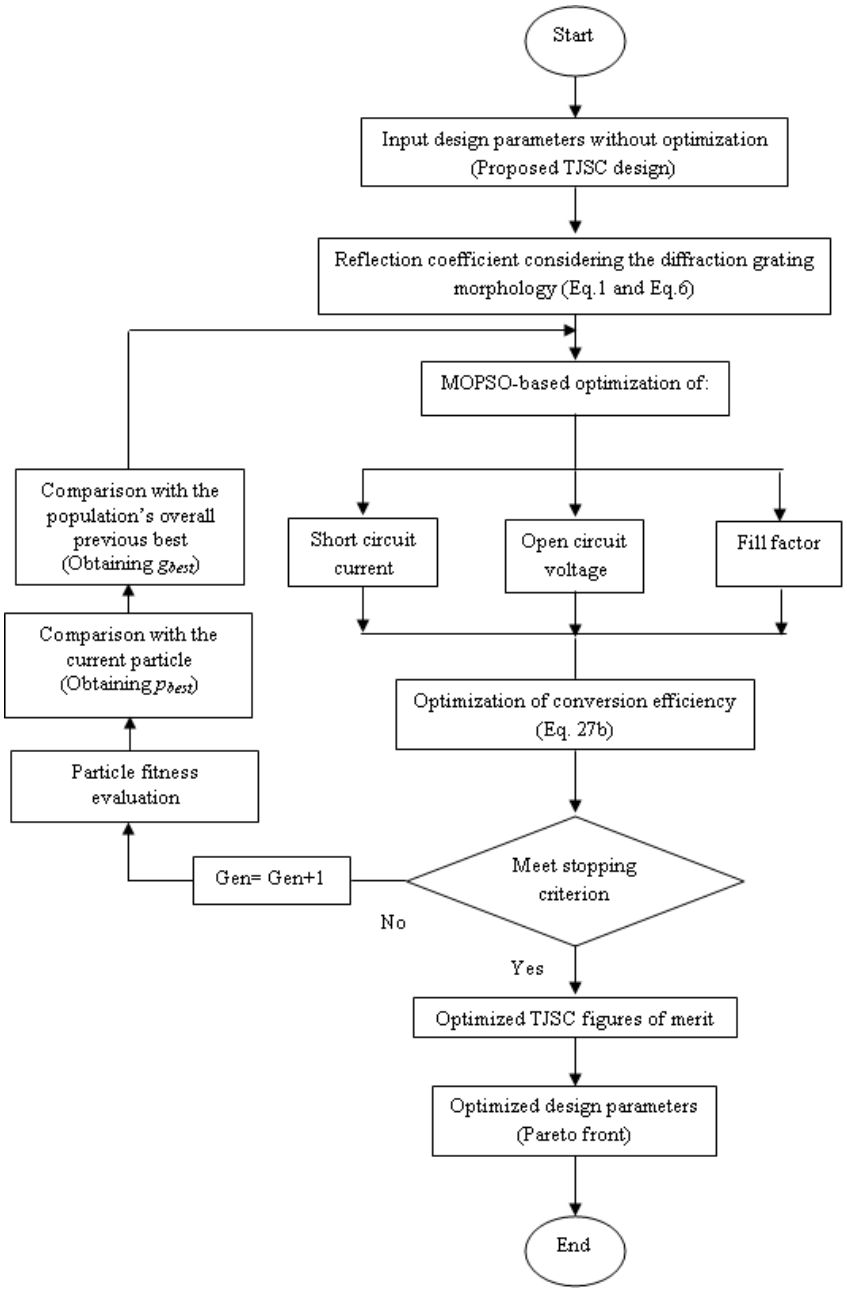


**Figure.9** Flowchart of the proposed MOPSO approach.

In this work, we deal with three objective functions, considered in the form of $J_{SC}$ , $V_{OC}$ and $FF$; where $Y = \{d, n, \psi_1, \psi_2, N_{A\text{-}GaAs}, N_{D\text{-}InGaP}, W_{n\text{-}InGaP}, W_{p\text{-}GaAs}, N_{A\text{-}BSF}, W_{BSF}, N_{A\text{-}Ge}, N_{D\text{-}Ge}, W_{n\text{-}Ge}, W_{p\text{-}Ge}\}$ are vector parameters of the device.

The assessment of design optimization is performed considering the following objective:

- Maximization of the short circuit current
- Maximization of the open circuit current

https://doi.org/10.1016/j.ijleo.2020.165346

- Maximization of the fill factor

The optimization procedure takes into consideration the physical and geometric parameters constraints of *Y* that relies to realistic values. The stopping criterion is attained when the fitness best quality is achieved or the result is unchangeable. When a termination criterion is reached a best (optimum) solution is located.

For the purpose of applying MOPSO approach on the proposed light trapping formalism, we present the obtained results for top sub cell GaInP/GaAs, single and bottom Ge solar cells. The MOPSO process of the adopted optimization approach considers a 100 as a size of population and 1000 as maximum number of generations. At the end of the optimization process all objective functions are stabilized. The MOPSO parameters change in a specific sweeping range linked to an optimization error. The best objective functions values are generated by means of Pareto solution in figure 10.

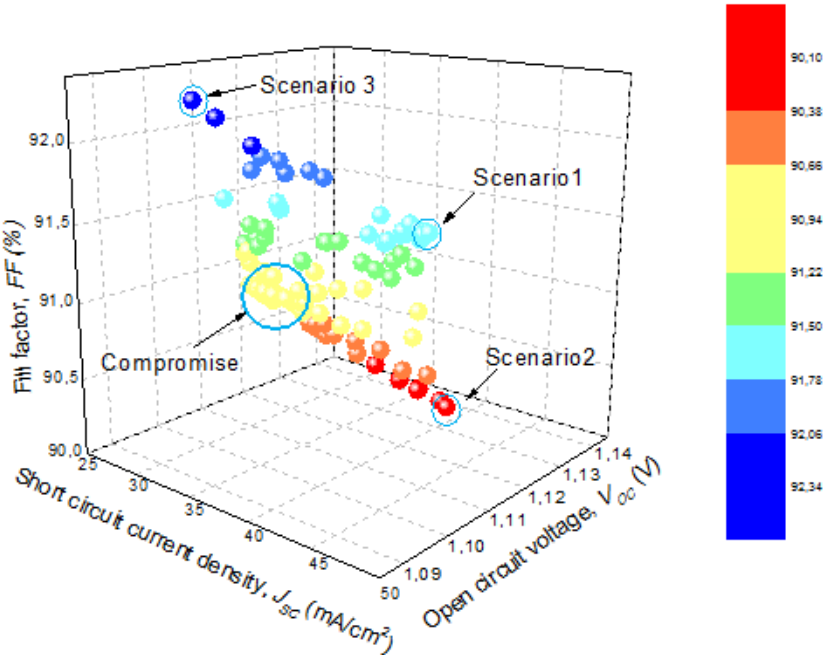


*(a)*

https://doi.org/10.1016/j.ijleo.2020.165346

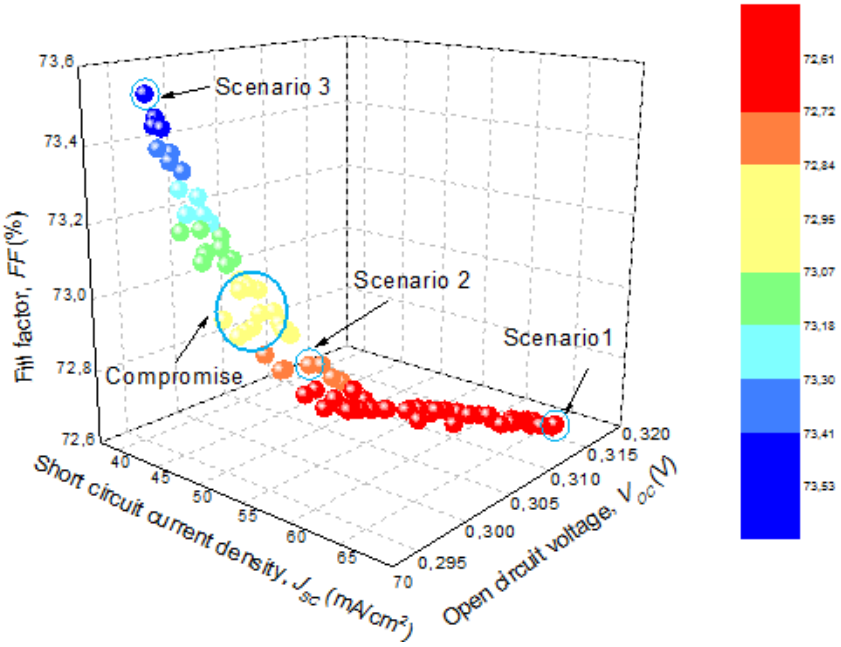


*(b)*

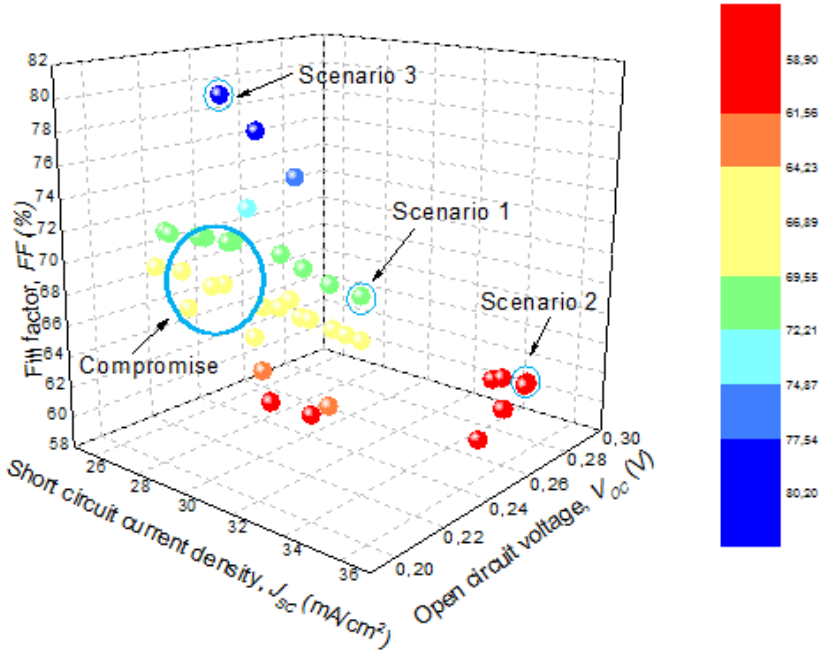


*(c)*

**Figure.10** Pareto-optimal solutions of the investigated solar cells. a) Top sub cell, b) Single Ge sub cell, c) Bottom Ge sub cell.

In this figure each point represents a single Pareto solution that describes the objective function's value furnished by a specific solar cell structure conception. Among multitude solutions a three solutions have been chosen for each solar cell (top, single and bottom) and the

best three scenarios parameters design (i.e. scenario1, scenario2, and scenario3) are listed in Table 6.

**Table.6** Pareto-optimal solutions parameters.

| | **Scenario 1** | **Scenario 2** | **Scenario 3** |
|---|---|---|---|
| **$In_{0.49}Ga_{0.51}P$/GaAs top sub cell** (figure 10-a) | | | |
| Short circuit current density, $J_{SC}$ (mA/cm$^2$) | **45** | 39.9 | 34.47 |
| Open circuit voltage $V_{oc}$(V) | 1.1 | **1.13** | 1.09 |
| Fill factor, *FF* (%) | 91.68 | 90.1 | **92.33** |
| Efficiency, $\eta$ (%) | 46.7 | 41.8 | 35.7 |
| **Single Ge sub cell** (figure 10-b) | | | |
| Short circuit current density $J_{SC}$ (mA/cm$^2$) | **66** | 49.75 | 41 |
| Open circuit voltage, $V_{oc}$ (V) | 0.315 | **0.3** | 0.295 |
| Fill factor, *FF* (%) | 72.6 | 72.8 | **73.5** |
| Efficiency, $\eta$ (%) | 15.5 | 11.2 | 9.15 |
| **Ge Bottom sub cell** (figure 10-c) | | | |
| Short circuit current density $J_{SC}$ (mA/cm$^2$) | **35.3** | 34.95 | 29.78 |
| Open circuit voltage, $V_{oc}$ (V) | 0.205 | **0.287** | 0.22 |
| Fill factor, *FF* (%) | 71.42 | 61.11 | **78.33** |
| Efficiency, $\eta$ (%) | 5.4 | 6.3 | 5.3 |

The versatility of Pareto solutions paves the way for designer to locate the suitable light trapping design for each sub cell. as an illustration, scenario1 for top, single and bottom sub cells show an improved values of the short circuit current, i.e. $J_{sc}$ = 45 mA, 66 mA and 35.3 mA; respectively. However, the rest of the objective function are slightly enhanced. This implies that, a superior improvement in the short circuit current can be reached by optimizing the light trapping parameters.

After the application of MOPSO approach on the top, single and bottom solar cells separately, targeting an ultimate best solution for the mechanically stacked tandem solar cell that establishes a compromise between all objective functions it basically goes through the "weighted sum approach method". The following expression describes the considered approach:

$$Fitness\ (Y) = w_1 J_{SC} + w_2 V_{OC} + w_3 FF \qquad (25)$$

https://doi.org/10.1016/j.ijleo.2020.165346

where $w_i$ (i = 1-3) represent the objective function weight with no articulation preferred ($w$= 1/3). In order to assess the influence of the light trapping geometry on the tandem solar cell electrical performance, the *J-V* characteristics of the proposed TJSC design with and without optimization are compared to the conventional design (Fig. 1-b). In this context, the achieved results are shown in Figure 11.

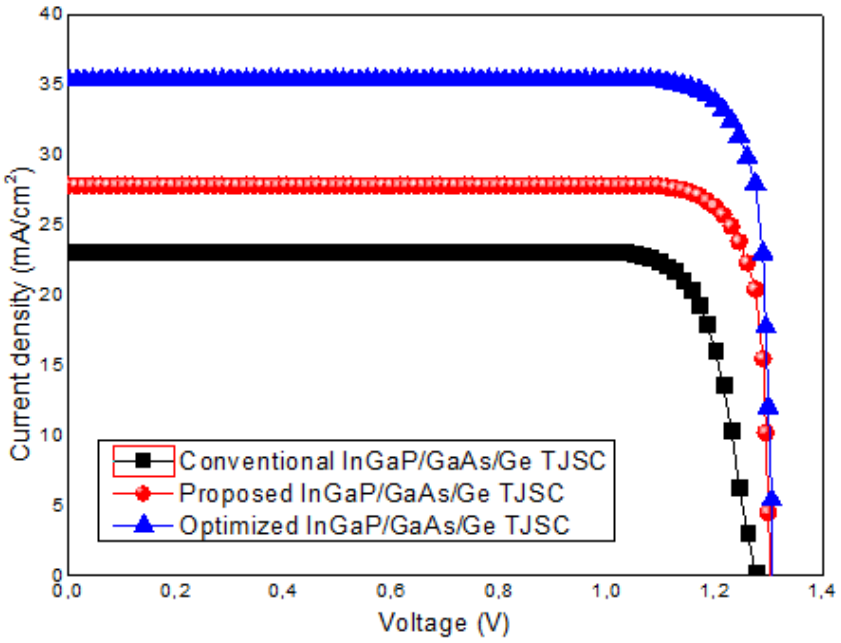


**Figure.11** Comparison between the proposed $In_{0.49}Ga_{0.51}P$/GaAs/Ge tandem solar cell with and without optimization and the conventional design.

From this figure, establishing an effective light trapping mechanism and BSF layer permits an improvement in both transmission and collection-separation mechanisms which in turn increase the conversion efficiency. Table 7 summarizes the comparison between the optimized and conventional TJSC solar cells. From this table, for a pyramid's angles of $\psi_1$=1.26 and $\psi_2$=0.5, an *ARC* refractive index and thickness of 1.85 and 60nm, the conversion efficiency rise to reach a maximum value around 41.7%. It is worth noticing that the value of ARC refractive index corresponds to the ZnO thin film.

https://doi.org/10.1016/j.ijleo.2020.165346

**Table.7** Comparison between the optimized and conventional TJSC solar cells.

| Design parameters | Experimental results [29] | Conventional tandem cell | Proposed tandem cell | Optimized tandem cell |
|---|---|---|---|---|
| **Light trapping design parameters** | | | | |
| *SLARC* Thickness, *d* (nm) | / | / | 30 | 60 |
| *SLARC* Refractive index, *n* | / | / | 1.6 | 1.85 (ZnO) |
| Angle of texturization, $\psi 1$ (top) | / | / | 1.2 | 1.26 |
| Angle of texturization, $\psi 2$ (bottom) | / | / | 1.2 | 0.5 |
| **Solar cell design parameters** | | | | |
| GaAs doping concentration, $N_a$ ($cm^{-3}$) | $10^{15}$-$10^{16}$ | $10^{16}$ | $10^{16}$ | $2\times10^{16}$ |
| InGaP doping concentration, $N_d$ ($cm^{-3}$) | $5\times10^{16}$-$5\times10^{18}$ | $10^{18}$ | $10^{18}$ | $5.5\times10^{18}$ |
| InGaP (n)region thickness, $W_n$ (µm) | 10 | 2 | 2 | 1.4 |
| GaAs (p)regionthickness, $W_p$ (µm) | 10 | 2 | 2 | 2.35 |
| GaAs (BSF) region thickness, $W_{BSF}$ (µm) | / | / | 0.5 | 0.3 |
| GaAs (BSF) doping concentration, $N_{aBSF}$ ($cm^{-3}$) | / | / | $10^{19}$ | $5\times10^{19}$ |
| Ge doping concentration, $N_a$ ($cm^{-3}$) | $10^{15}$-$10^{16}$ | $10^{16}$ | 1016 | $10^{17}$ |
| Ge doping concentration, $N_d$ ($cm^{-3}$) | $10^{18}$-$10^{19}$ | $10^{19}$ | $10^{19}$ | $3\times10^{19}$ |
| Ge (n)region thickness, $W_n$ (µm) | 20 | 20 | 20 | 20 |
| Ge (p)region thickness, $W_p$ (µm) | 130 | 130 | 130 | 130 |
| **Objective functions** | | | | |
| Short circuit current, $J_{SC}$ ($mA/cm^2$) | 12.6 | 23.3 | 28 | 35.3 |
| Open circuit voltage, $V_{oc}$ (V) | 2.13 | 1.28 | 1.288 | 1.305 |
| Fill factor, *FF* (%) | 60 | 83 | 87.7 | 88 |
| maximum power density | 16.1 | 24.75 | 31.6 | 40.5 |
| Efficiency, $\eta$ (%) | 16.5 | 25.5 | 32.5 | 41.7 |

Table 7 summarize the optimized design parameters of the proposed mechanically stacked tandem solar cell, considering the textured morphology formalism, antireflection coating and the BSF layer, Our finding proves the outstanding results reached when applying the proposed methodology that combines an improved light trapping mechanism with a metaheuristic MOPSO approach. The proposed design methodology permits to surpass surprisingly the conventional structure.

https://doi.org/10.1016/j.ijleo.2020.165346

## Conclusion

In this work, the role of light trapping mechanism in improving InGaP/GaAs/Ge tandem solar cell electrical and optical performances has been analytically investigated. Comprehensive analytical model, which can describe the device behavior including the optical confinement effect, have been developed focusing on the device conversion capability optimization. Also, using single antireflection coating and back surface field aspects at top cell has a meaning impact on the device performance, which allows the improvement of the electrical and optical performance. The lowering of the surface reflection is a key factor in improving the light conversion capability. In order to boost the device performance, a MOPSO-based optimization approach has been successfully implemented in the context of our investigation, where the optimized design outperforms considerably the conventional designs.

**Acknowledgements**

This work was supported by DGRSDT Of Ministry of Higher education of Algeria. The work was done in the unit of research of materials and renewable energies (URMER).

## References


[1] Green, M. A., Dunlop, E. D., Levi, D. H., Hohl-Ebinger, J., Yoshita, M., & Ho-Baillie, A. W. Solar cell efficiency tables (version 54). Progress in Photovoltaics: Research and Applications, vol. 27(7), pp. 565-575, 2019. doi:10.1002 /pip.3171.

[2] M. Yamaguchi. "III-V compound multi-junction solar cells: present and future". Sol Energy Mater Sol Cells, vol 75 (1-2), pp. 261-269, 2003. doi: 10.1016/S0927-0248(02)00168-X.

[3] Research Cell Efficiency Records, [online] Available: https://www.nrel.gov/pv/cell-efficiency.html.

[4] J. F. Geisz, , R. M. France, K. L. Schulte, M.A Steiner, A. G. Norman, H. L. Guthrey, T. Moriarty. "Six-junction III–V solar cells with 47.1% conversion efficiency under 143 Suns concentration". Nature Energy, pp. 1-10, 2020.

[5] T. Takamoto, E. Ikeda, H. Kurita, M. Ohmori, M. Yamaguchi and M.J. Yang, "Two-Terminal Monolithic In0.5Ga0.5P/GaAs Tandem Solar Cells with a High Conversion Efficiency of Over 30%". Japan. J. Appl. Phys. Vol. 36, pp. 6215, 1997. doi: 10.1143/JJAP.36.6215.

[6] A W. Bett, F. Dimroth, G. Stollwerck and O V. Sulima, "III-V compounds for solar cell applications". Appl. Phys. A, vol. 69, pp. 119, 1999. doi: 10.1007/s003390050983.

[7] Yamaguchi M et al, "Novel materials for high-efficiency III–V multi-junction solar cells", Sol. Energy. vol. 82, pp. 173, 2008. doi: 10.1016/j.solener.2007.06.011.

[8] M D. Yang, Y K. Liu, J L. Shen, C H. Wu, C A. Lin, W H. Chang, H H. Wang, H I. Yeh, W H. Chan and W J. Parak, "Improvement of conversion efficiency for multi-junction solar cells by incorporation of Au nanoclusters". Opt. Express. vol. 16, Issue 20, pp. 15754-15758, 2008, doi: 10.1364/OE.16.015754.

[9] P. Matheu, S H. Lim, D. Derkacs, C. McPheeters and E T. Yu, "Nanophotonic light trapping in solar cells".Appl. Phys. Lett. vol. 93, pp. 108-113, 2008. doi: 10.1063/1.4747795.

[10] J. Zhao, A. Wang, M A. Green and F. Ferrazza, "19.8% efficient "honeycomb" textured multicrystalline and 24.4% monocrystalline silicon solar cells". Appl. Phys. Lett. Vol. 73, pp. 1991, 1998. doi: 10.1063/1.122345.

[11] J.F. Geisz, D.J. Friedman, J.S. Ward, A. Duda, W.J. Olavarria, T.E. Moriarty, J.T. Kiehl, M.J. Romero, A.G. Norman, K.M. Jones, "40.8% efficient inverted triple-junction solar cell with two independently metamorphic junctions". Appl. Phys. Lett. vol. 93, pp. 123505, 2008. doi: 10.1063/1.2988497.

[12] J. E. Alvarez-Benitez, R. M. Everson, J. E. Fieldsend. "A MOPSO algorithm based exclusively on pareto dominance concepts". In International Conference on Evolutionary Multi-Criterion Optimization", pp. 459-473, 2005Springer, Berlin, Heidelberg. doi: 10.1007/978-3-540-31880-4_32.

[13] F. Rezaei, H. R. Safavi, A. Mirchi, K. Madani. "f-MOPSO: An alternative multi-objective PSO algorithm for conjunctive water use management". Journal of Hydro-environment Research, vol. 14, pp.1-18. doi: 10.1016/j.jher.2016.05.007.

[14] L. Jia, D. Cheng, M. S. Chiu. "Pareto-optimal solutions based multi-objective particle swarm optimization control for batch processes". Neural Computing and Applications, vol. 21(6), pp. 1107-1116, 2012. doi: 10.1007/s00521-011-0659-6.

[15] A. Yousfi, Z. Dibi, S. Aissi, H. Bencherif, L. Saidi. "RF/analog performances enhancement of short channel GAAJ MOSFET using source/drain extensions and metaheuristic optimization-based approach". Journal of Telecommunication, Electronic and Computer Engineering (JTEC), vol. 10(2), pp. 81-90, 2018.

[16] M. Yamamoto, "Surface plasmon resonance (SPR) theory: tutorial. Review of Polarography", vol. 48(3), pp. 209-237, 2002. doi: 10.5189/revpolarography.48.209.
[17] M. Born, E. Wolf, "Principles of optics: electromagnetic theory of propagation, interference and diffraction of light". Elsevier, 2013.
[18] L. Wu, H. S. Chu, W. S. Koh, E. P. Li, "Highly sensitive graphene biosensors based on surface plasmon resonance", Optics express, vol. 18(14), pp. 14395-14400, 2010. doi: 10.1364/OE.18.014395.
[19] H. Bencherif, L. Dehimi, F. Pezzimenti, F.G. Della Corte, "Improving the efficiency of a-Si: H/c-Si thin heterojunction solar cells by using both antireflectioncoating engineering and diffraction grating". Optik, vol. 182, pp. 682–693, 2019. doi: 10.1016/j.ijleo.2019.01.032.
[20] W.J. Yang, Z.Q. Ma, X. Tang, C.B. Feng, W.G. Zhao, P.P. Shi, "Internal quantum efficiency for solar cells". Sol. Energy, vol. 82, pp. 106–110, 2008. doi: 10.1016/j.solener.2007.07.010.
[21] S. M. Sze, K. K. Ng. "Physics of semiconductor devices". John wiley & sons, 2006.
[22] M. Krichen, A. B.Arab. "Analytical study of a-Si: H/c-Si thin heterojunction solar cells with back surface field". Journal of Computational Electronics, vol. 15(1), pp. 269-276. doi: 10.1007/s10825-015-0756-3.
[23] R. A. Wind, H. Jones, M. J. Little, M. A. Hines, "Orientation-resolved chemical kinetics: using micro fabrication to unravel the complicated chemistry of KOH/Si etching". The Journal of Physical Chemistry B, vol. 106(7), pp. 1557-1569, 2002. doi: 10.1021/jp011361j.
[24] M. Reyes-Sierra, C.C. Coello, et al, "Multi-objective particle swarm optimizers: A survey of the state-of-the-art". Int. J. Comput. Intelligence Res. vol2 (3), pp. 287–308, 2006. doi: 1.5019/j.ijcir.2006.68.
[25] S. Mostaghim, J. Teich, "Strategies for finding good local guides in multi- objective particle swarm optimization (MOPSO)". in: Swarm Intelligence Symposium, SIS'03. Proceedings of the IEEE, pp. 26–33. 2003. doi: 10.1109/SIS.2003.1202243.
[26] H. Bencherif, L. Dehimi, F. Pezzimenti, G. De Martino, F. G. Della Corte, "Multiobjective Optimization of Design of 4H-SiC Power MOSFETs for Specific Applications". Journal of Electronic Materials, vol. 48(6), pp. 3871-3880, 2019. doi: 10.1007/s11664-019-07142-5.
[27] F. Pezzimenti, H. Bencherif, A. Yousfi, L. Dehimi, "Current-voltage analytical model and multiobjective optimization of design of a short channel gate-all-around-junctionless MOSFET. Solid-State Electronics, vol. 161, pp. 107642. doi: 10.1016/j.sse.2019.107642.
[28] H. Bencherif, L. Dehimi, G. Messina, P. Vincent, F. Pezzimenti, F. G. Della Corte. "An optimized Graphene/4H-SiC/Graphene MSM UV-photodetector operating in a wide range of temperature". Sensors and Actuators A: Physical, 112007. doi: 10.1016/j.sna.2020.112007.
[29] S. Yoshidomi, J. Furukawa, M. Hasumi, and T. Sameshima, "Mechanical Stacking Multi Junction Solar Cells Using Transparent Conductive Adhesive". Energy Procedia vol. 60, p. 116, 2014. doi: 10.1016/j.egypro.2014.12.352.